

Supporting Information

Scalable Fabrication of Kevlar/Ti₃C₂T_x MXene Intelligent Wearable Fabrics with Multiple Sensory Capabilities

*Baochang Cheng,¹ and Peiyi Wu^{1,2} **

¹State Key Laboratory of Molecular Engineering of Polymers, Department of Macromolecular Science and Laboratory of Advanced Materials, Fudan University, Shanghai 200433, PR China.

²State Key Laboratory for Modification of Chemical Fibers and Polymer Materials, College of Chemistry, Chemical Engineering and Biotechnology, Center for Advanced Low-Dimension Materials, Donghua University, Shanghai 201620, PR China.

E-mail: peiyiwu@fudan.edu.cn

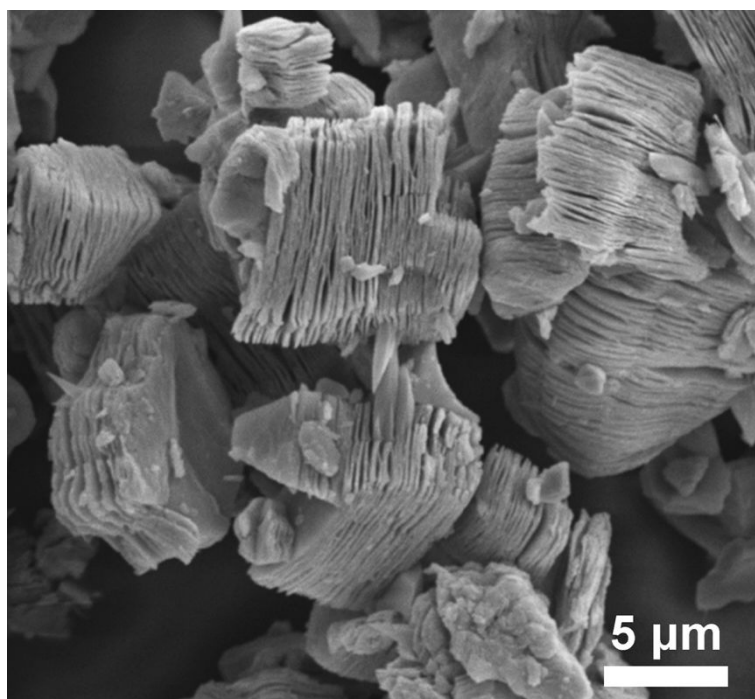


Figure S1. SEM image of the Ti₃AlC₂ MAX. A typical accordion-like structure can be seen clearly.

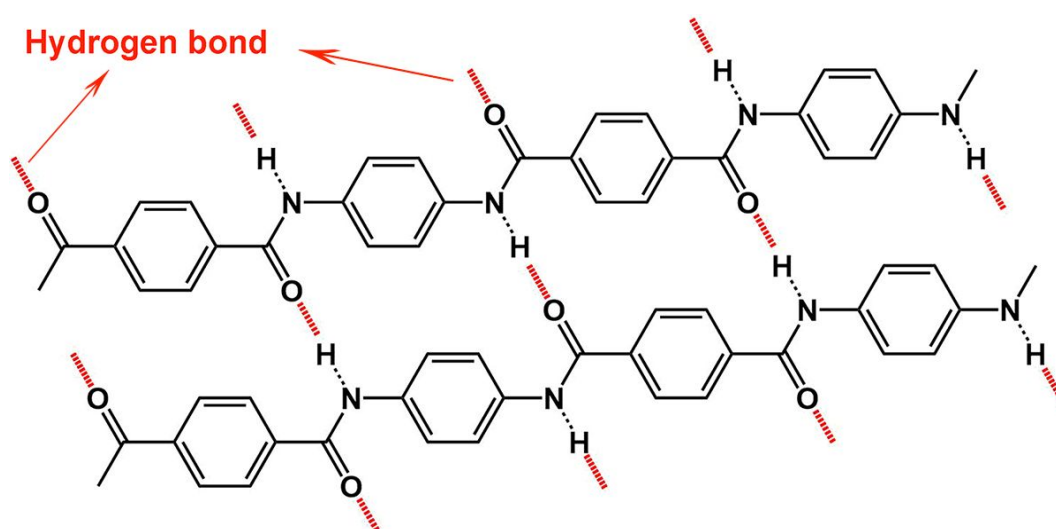


Figure S2. Single Kevlar fiber consists of aligned poly (*p*-phenylene terephthalamide) molecular chains connected by hydrogen bonds.

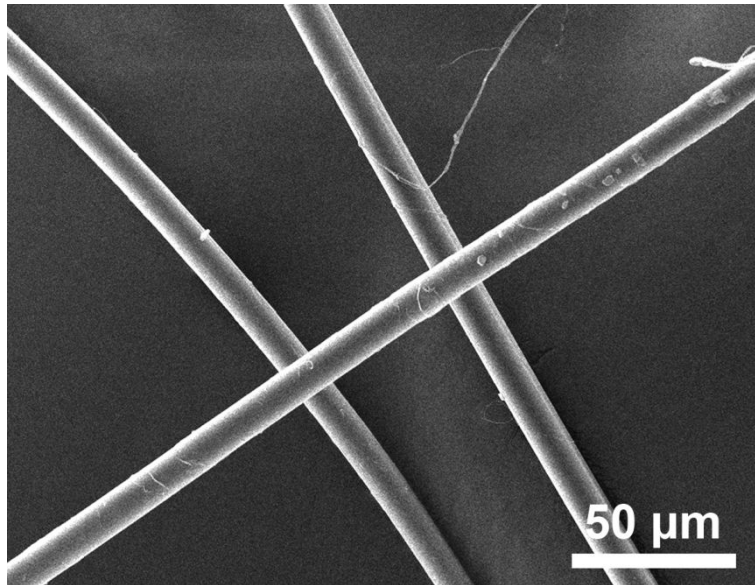


Figure S3. SEM image of the Kevlar fiber with an average diameter of nearly 11 μm .

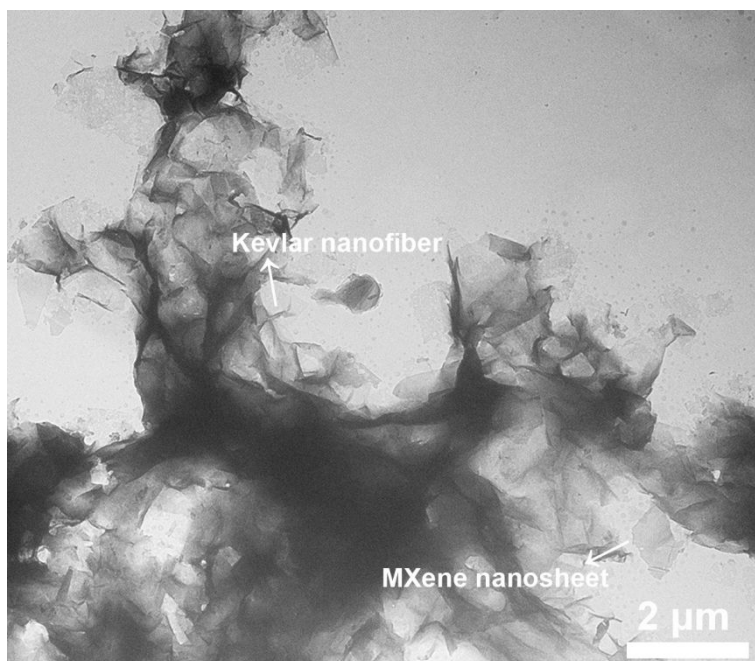


Figure S4. TEM image of the KM mixed solution. It exhibits homogeneous coexisting microstructures of Kevlar nanofibers and MXene nanosheets.

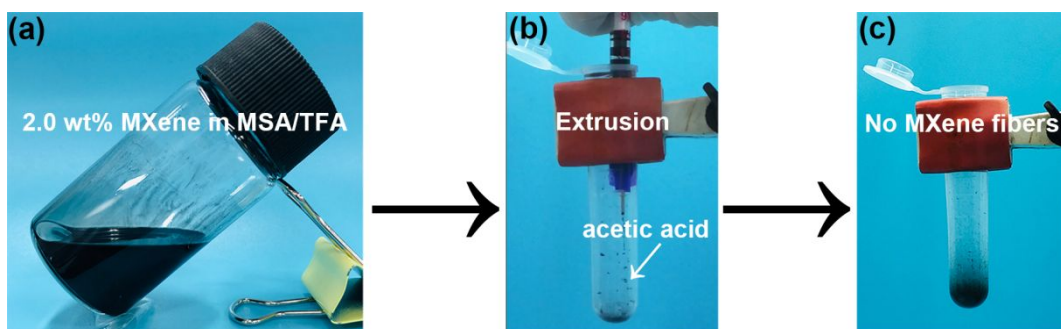


Figure S5. Photographs showing the extrusion process of pure MXene (2.0 wt%) acid solution. The result indicates that the pure MXene acid solution could not form fibers *via* wet-spinning.

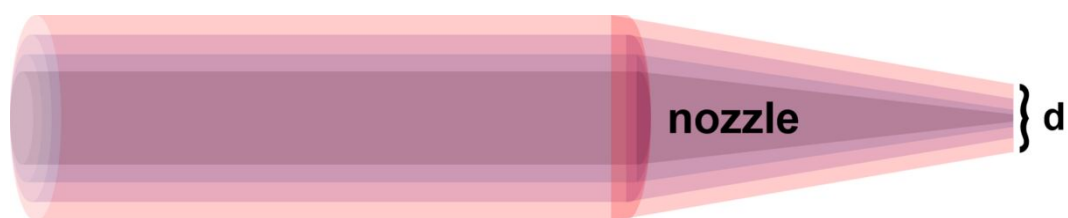


Figure S6. A cartoon diagram illustrates the mechanism of the adjustable diameters of KM fibers. “d” presents the diameter of the nozzle, it can be regulated from 0.11 to 0.16, 0.21, 0.34, 0.41, 0.51, 0.60 and 0.84 mm easily.

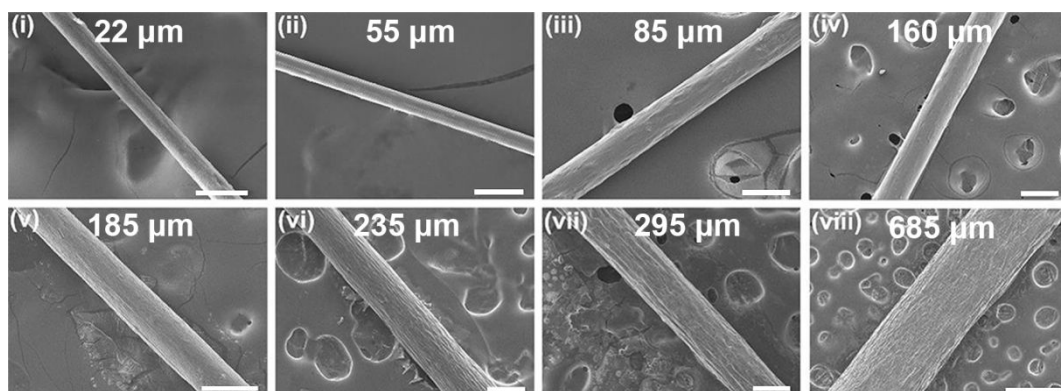


Figure S7. SEM images of KM fibers with adjustable diameters from 22 to 685 μm were prepared through extruding with different sizes of the nozzle (i-viii). Scale bar = 50 μm for i, 100 μm for ii-iii, 200 μm for iv-vii and 500 μm for viii.

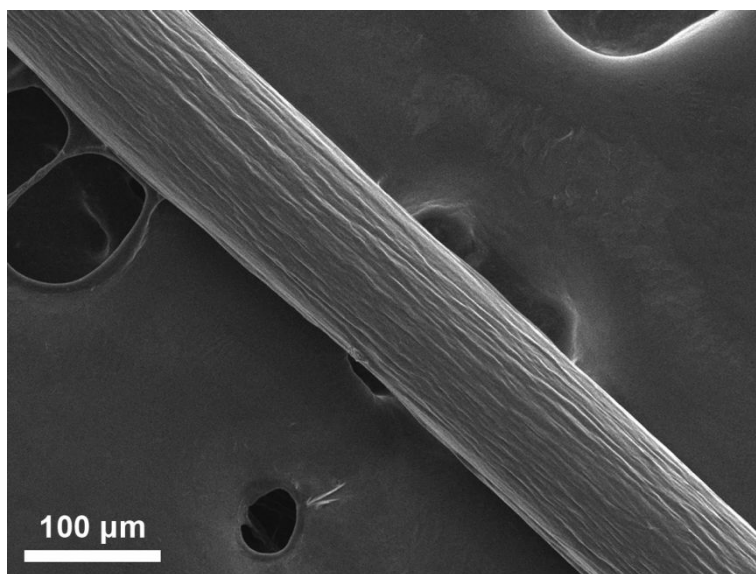


Figure S8. SEM image of a regenerated Kevlar hydrogel fiber with a concentration of 1.0 wt%. The surface of the fiber is smooth and the diameter is homogeneous.

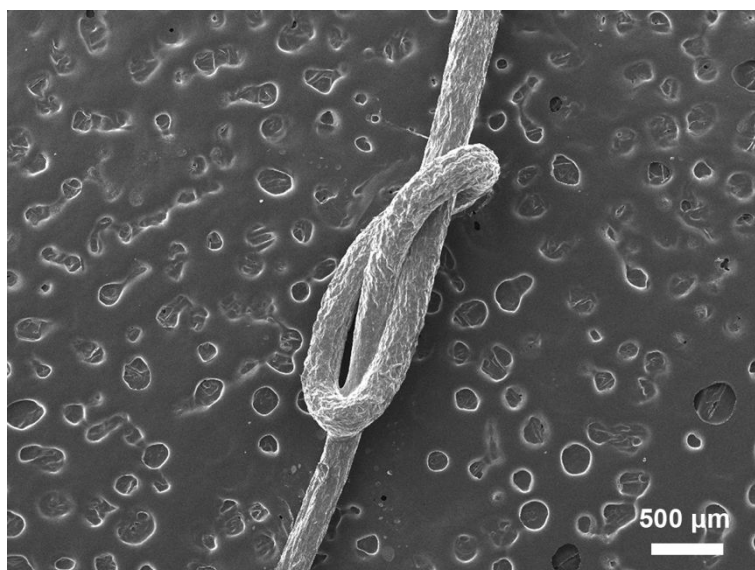


Figure S9. SEM image of a knotted K_1M_1 fiber with a MXene loading of 1.0 wt%, this result demonstrates the high flexibility of K_1M_1 fiber.

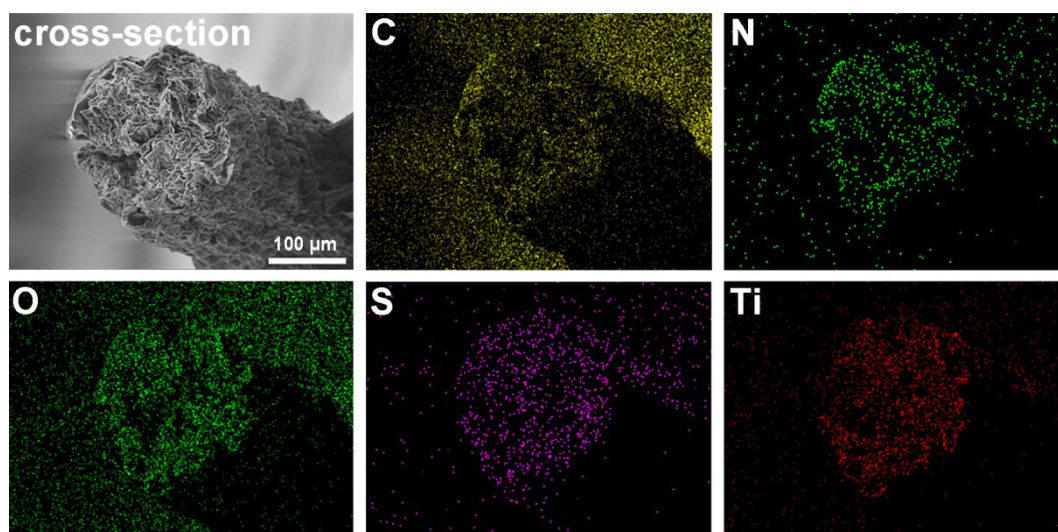


Figure S10. Cross-section SEM image and corresponding EDX mapping of K_1M_1 fiber.

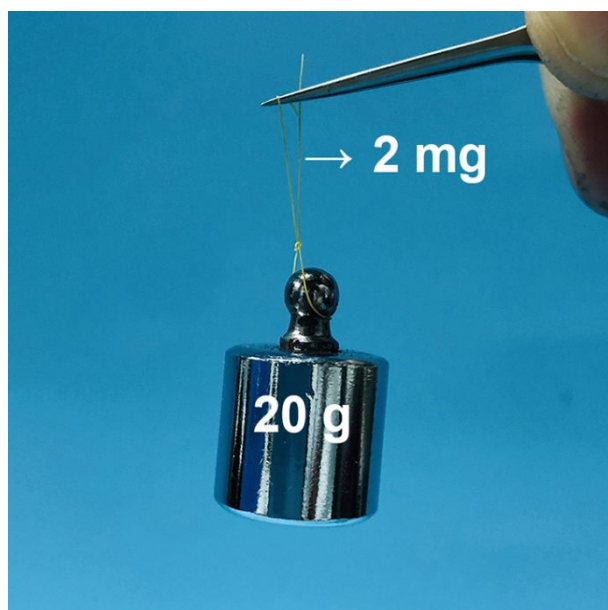


Figure S11. A regenerated Kevlar hydrogel fiber (1.0 wt%) of 2 mg can lift up a weight of 20 g which is 10000 times heavier than the fiber.

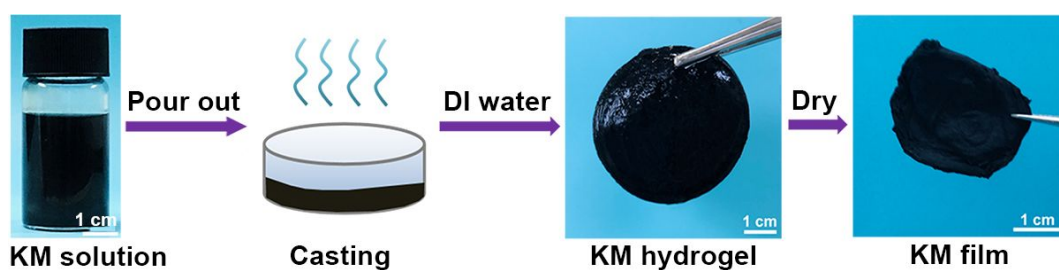


Figure S12. A typical solution-hydrogel-film transformation of Kevlar/MXene mixed acid solution. A bottle of KM acid solution (~5 mL) was poured out and casted into a plastic dish (diameter = 6 cm), followed by distilled water exchanging for the conversion of KM hydrogel. And then, the KM hydrogel was dried at room temperature and transformed into a black KM film.

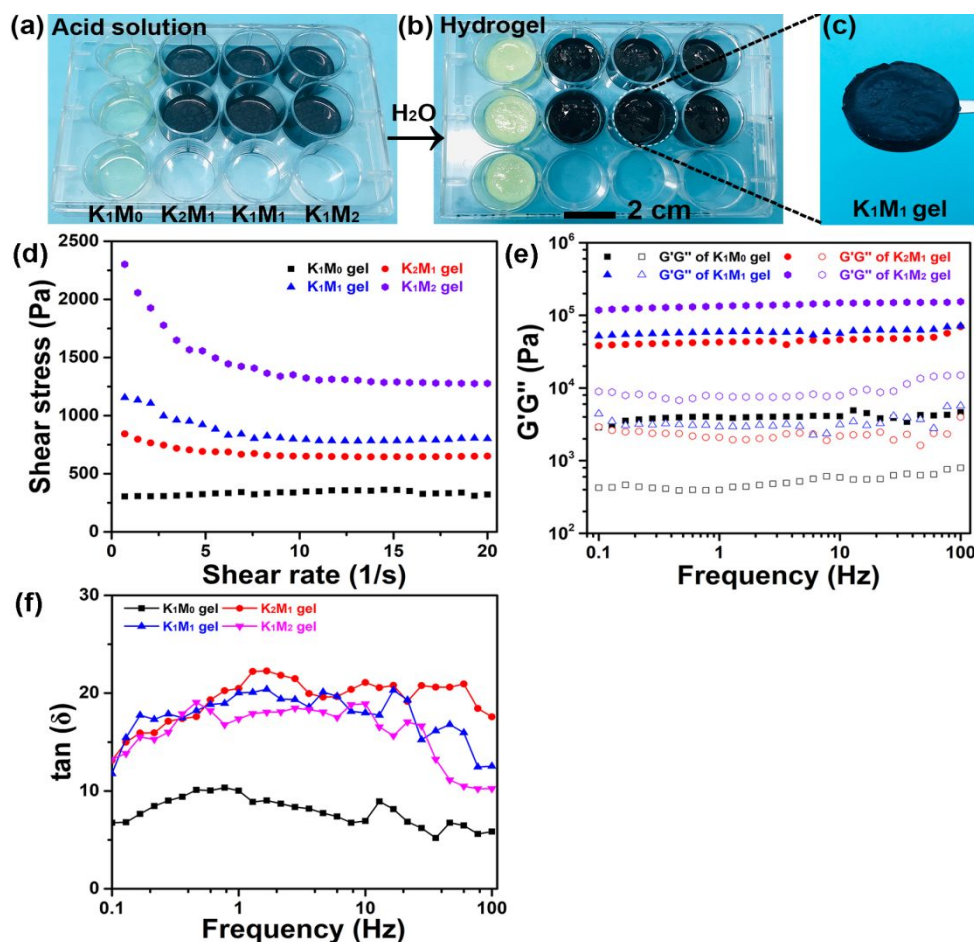


Figure S13. The Sol-Gel transition process of KM composites and rheological analysis. (a) Acid solutions of KM composites. (b) KM composite hydrogels. (c) Enlarged image of the K_1M_1 hydrogel. Rheology analysis of (d) Shear rate sweep and (e) Frequency sweep and (f) Tangential loss angle ($\tan \delta$) at frequency sweep mode of the prepared hydrogels.

According to the results, KM composite acid solutions can be transformed into KM composite hydrogels with the aid of H_2O easily. For shear rate sweep, with the MXene concentration increasing, K_1M_2 hydrogel exhibits higher shear stress than other KM composite hydrogels with low concentrations of MXene. And KM hydrogels show progressive increment of the G' and G'' moduli with the increasing of MXene due to its reinforcement.

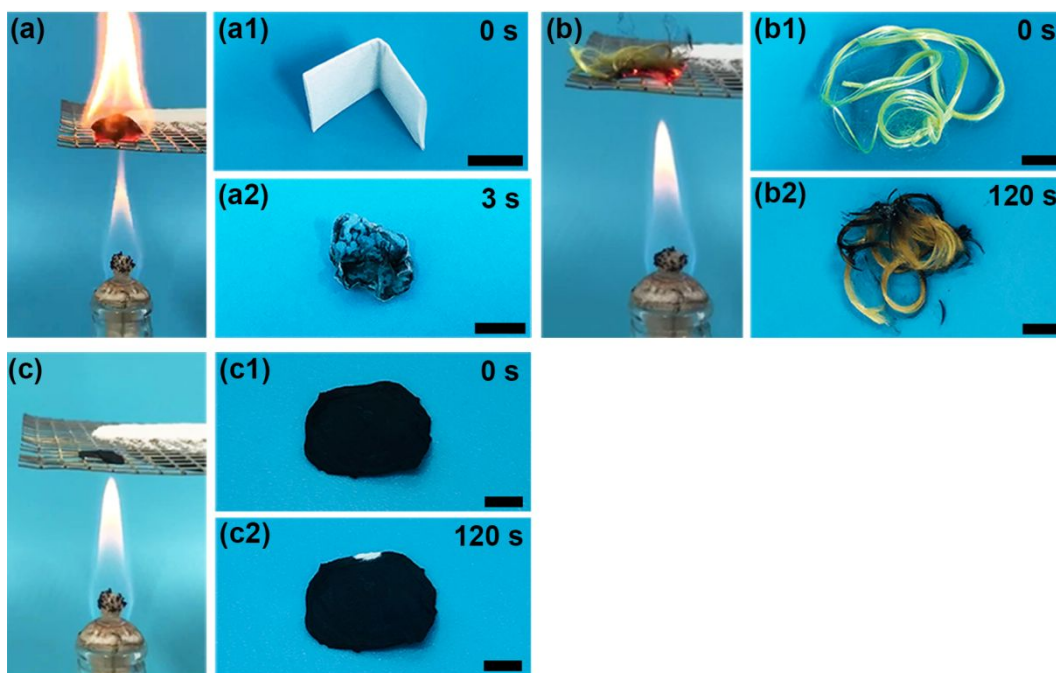


Figure S14. Video captures of the burning results of (a) cellulose filter paper, (b) Kevlar fiber and (c) KM film. a1, b1, c1 and a2, b2, c2 are the corresponding status of before and after burning. The weight of cellulose filter paper, Kevlar fiber and KM film is 60 mg. Scale bar = 1 cm.

As shown in Figure S14, the combustion processes of the same weight (~ 60 mg) of cellulose filter paper (Figure S14-a), Kevlar fiber (Figure S14-b) and K_1M_1 film (Figure S14-c) were proved detailedly. Cellulose filter paper, with a main component of cellulose based fiber, holds a representative flammable characteristic. Under burning with an alcohol lamp, the cellulose filter paper was burned into ashes within 2 seconds (Supporting Video S3, Supporting Information), showing an extremely flammable property. As a high performance composite fiber, Kevlar has a preeminent fire resistance. As shown in Figure S14-b, an improved fire resistance of Kevlar fiber was observed. As recorded in Supporting Video S4 (Supporting Information), only

part of the surface of the Kevlar fiber was carbonized after 120 seconds burning, suggesting the inherent fire resistance performance. The introduction of MXene, endows the KM composites with an enhanced flame resistance and thermal stability. On account of the synergistic enhancement effect of Kevlar and MXene, the fire resistance is improved. As shown in Figure S12, a KM film was prepared with a solution-hydrogel-film transformation. K_1M_1 film kept a high degree of structural integrity after a quite long-term ignition (Supporting Video S5, Supporting Information). Just only a small edge of the surface was carbonized due to the concentrated high temperature baking. SEM images of the surface of K_1M_1 film before and after burning also show a relatively complete micromorphology (Figure S15, Supporting Information). These results indicate that the KM composites possess an enhanced flame resistance and thermal stability which can be used in numerous complex and harsh environments, such as fire rescuing, fire prevention apparatus and space exploration.

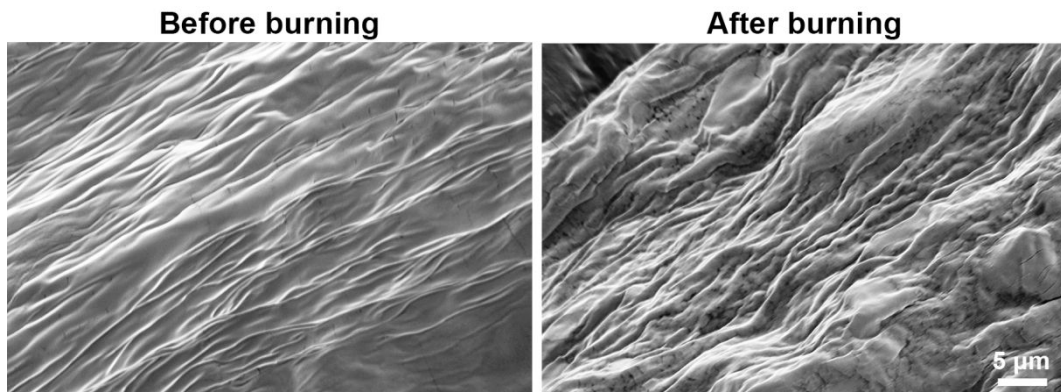


Figure S15. SEM images of K_1M_1 film before and after burning.

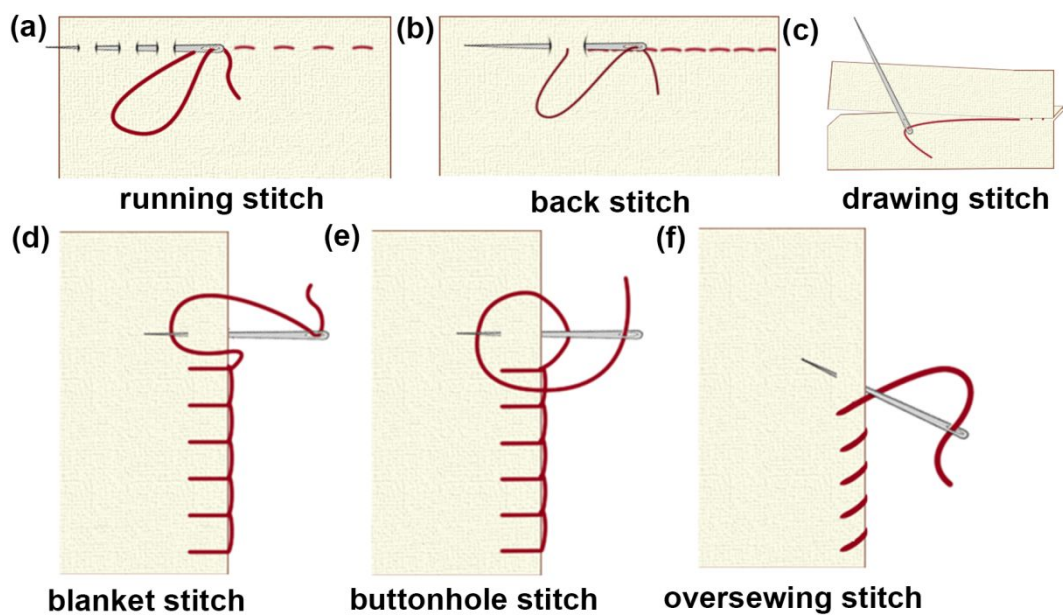


Figure S16. Particular skills and elaborate designs in the fabrication processes of the “Chinese sewing craftsmanship”.

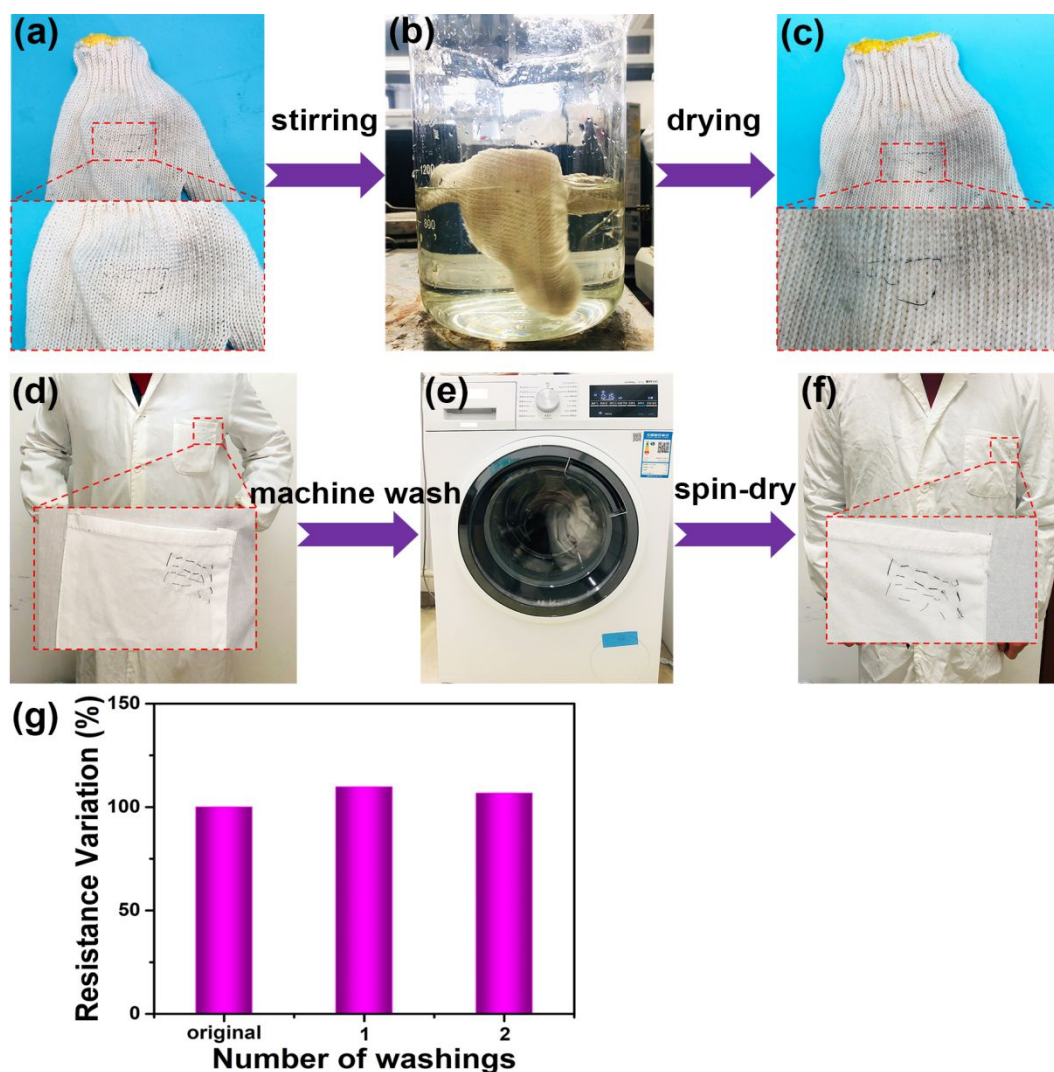


Figure S17. Washability tests of KM fiber based sensors with different procedures. (a-c) Washing by a washing machine with a common washing procedure. (d-f) Simulated washing by continuous stirring. (g) Resistance variation of KM fiber based sensor before and after several times of washing. The sensors can keep its original shapes and maintain the electrical properties after several times of washing.

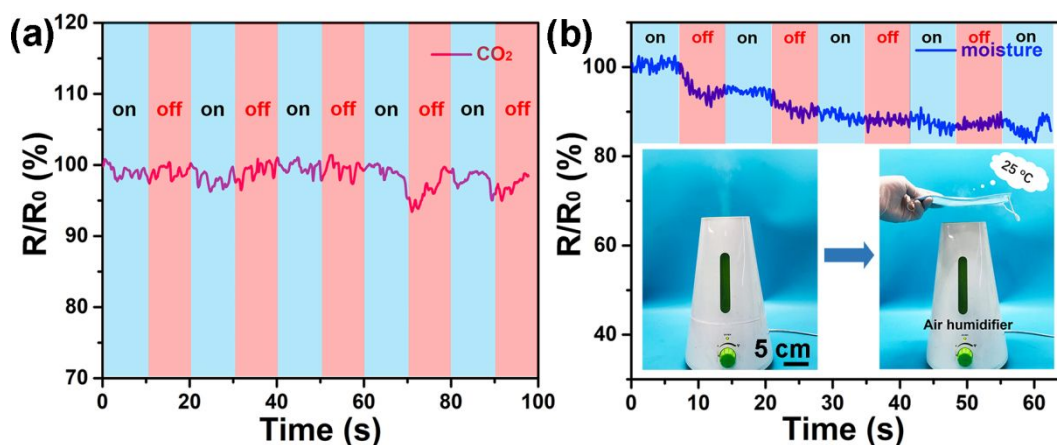


Figure S18. The irregular signals in respiratory monitoring under the influence of (a) CO₂ and (b) H₂O, respectively.

In order to eliminate the interference of H₂O and CO₂, we tested the influence caused by H₂O and CO₂ in the sensing procedures, especially in respiratory monitoring (For other signal tests, due to the protection of VHB tapes, the influence of H₂O and CO₂ can be ignored). An air humidifier was used to simulate the stable formation of H₂O with a temperature about 25 °C which is close to room temperature. This simulation process means the temperature variation is approximately zero, and also eliminates the interference of H₂O in the process of inhalation and exhalation. An intermittent stream of CO₂ was employed to imitate the influence of airflow during exhalation process. As results shown in Figure S18, the signal changes are irregularly in respiratory monitoring under the influence of H₂O and CO₂, indicating that the influence H₂O and CO₂ are negligible and can be ignored.

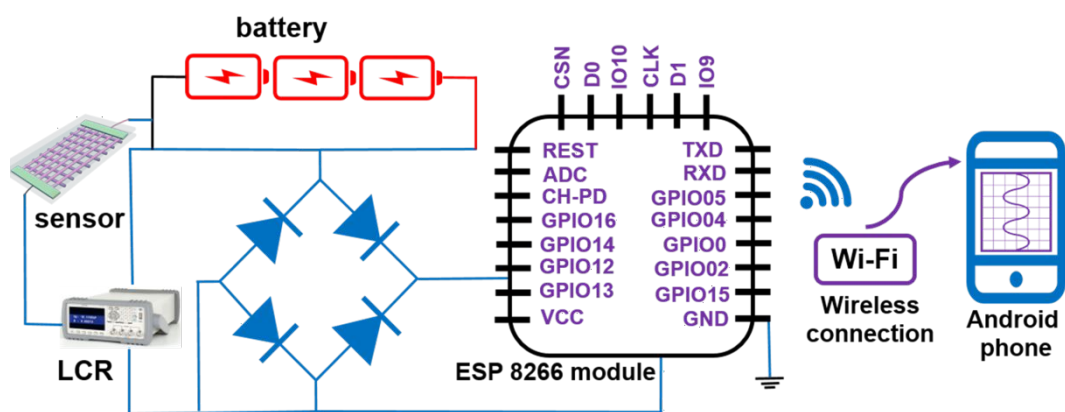


Figure S19. A circuit diagram of the wireless touch sensing system.

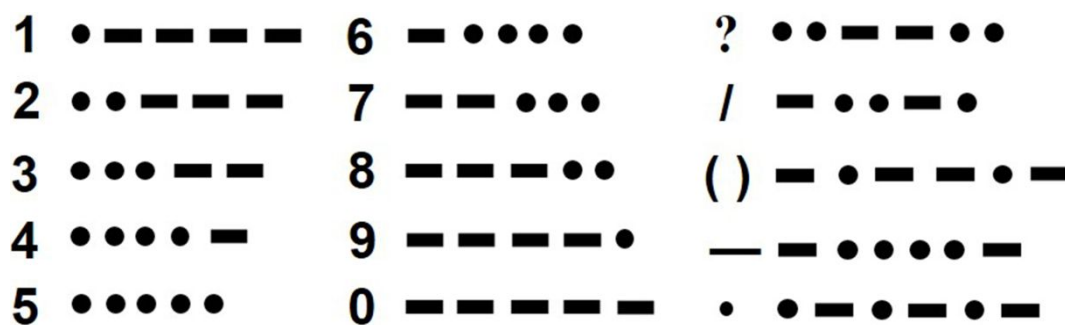


Figure S20. The corresponding Arabic numerals and other special symbols in the Morse code.

Table S1. The performance summary of KM fibers.

| Samples | Kevlar (wt %) | MXene (wt %) | Strain to break (%) | Young's modulus (GPa) | Conductivity (S m ⁻¹) |
|-------------------------------|------------------|-----------------|------------------------|--------------------------|--------------------------------------|
| K ₁ M ₀ | 1.0 | 0.0 | 15.54 | 0.415 | 0.979 |
| K ₂ M ₁ | 1.0 | 0.5 | 7.51 | 0.395 | 5.34 |
| K ₁ M ₁ | 1.0 | 1.0 | 6.35 | 0.751 | 11.28 |
| K ₁ M ₂ | 1.0 | 2.0 | 3.04 | 1.736 | 17.19 |

Table S2. A comparison between KM fiber based sensor and existing related works in terms of the sensitivity of temperature responding.

| Materials | Temperature range (°C) | Sensitivity (-% °C ⁻¹) | References |
|---|------------------------|------------------------------------|------------------|
| Silk-nanofiber-derived carbon fiber membranes | 25-80 | 0.81 | 1 |
| Graphene/polyurethane fiber | 20-100 | 0.815 | 2 |
| PDA/MXene/PDMS fiber | 25-100 | 0.7-1.8 | 3 |
| ZnO NW/PU fiber | 25-50 | 16.8-39.3 | 4 |
| SWCNTs based fiber | 30-80 | 1.95 | 5 |
| PUN hydrogel | 40-110 | 1.64 | 6 |
| Ag NFs/Ag NWs electrode | 30-45 | 0.03 | 7 |
| CNT/PEDOT:PSS film | 20-80 | 0.25 | 8 |
| Kevlar/MXene fiber | 10-60 | 0.77 | This work |

Supporting Video S1. K₁M₁ fiber was prepared by wet-spinning.

Supporting Video S2. The extrusion process of pure MXene (2.0 wt%) acid solution.

Supporting Video S3. The combustion process of cellulose filter paper.

Supporting Video S4. The combustion process of Kevlar fiber.

Supporting Video S5. The combustion process of K₁M₁ film.

Supporting Video S6. Remote real-time translation of the Morse code “SAVE ME” *via* a wireless controller with high quality and accuracy.

References:

- (1) Wang, C.; Xia, K.; Zhang, M.; Jian, M.; Zhang, Y., An All-Silk-Derived Dual-Mode E-Skin for Simultaneous Temperature-Pressure Detection. *ACS Appl. Mater. Interfaces* **2017**, *9*, 39484-39492.
- (2) Hu, X.; Tian, M.; Xu, T.; Sun, X.; Sun, B.; Sun, C.; Liu, X.; Zhang, X.; Qu, L., Multiscale Disordered Porous Fibers for Self-Sensing and Self-Cooling Integrated Smart Sportswear. *ACS Nano* **2020**, *14*, 559-567.
- (3) Luo, J.; Gao, S.; Luo, H.; Wang, L.; Huang, X.; Guo, Z.; Lai, X.; Lin, L.; Li, R. K. Y.; Gao, J., Superhydrophobic and Breathable Smart MXene-Based Textile for Multifunctional Wearable Sensing Electronics. *Chem. Eng. J.* **2021**, *406*, 126898.
- (4) Liao, X.; Liao, Q.; Zhang, Z.; Yan, X.; Liang, Q.; Wang, Q.; Li, M.; Zhang, Y., A Highly Stretchable ZnO@Fiber-Based Multifunctional Nanosensor for Strain/Temperature/UV Detection. *Adv. Funct. Mater.* **2016**, *26*, 3074-3081.
- (5) Zhao, J.; Zhang, Y.; Huang, Y.; Xie, J.; Zhao, X.; Li, C.; Qu, J.; Zhang, Q.; Sun, J.; He, B.; Li, Q.; Lu, C.; Xu, X.; Lu, W.; Li, L.; Yao, Y., 3D Printing Fiber Electrodes for an All-Fiber Integrated Electronic Device *via* Hybridization of an Asymmetric Supercapacitor and a Temperature Sensor. *Adv. Sci.* **2018**, *5*, 1801114.
- (6) Ge, G.; Lu, Y.; Qu, X.; Zhao, W.; Ren, Y.; Wang, W.; Wang, Q.; Huang, W.; Dong, X., Muscle-Inspired Self-Healing Hydrogels for Strain and Temperature Sensor. *ACS Nano* **2020**, *14*, 218-228.
- (7) An, B. W.; Heo, S.; Ji, S.; Bien, F.; Park, J.-U., Transparent and Flexible Fingerprint Sensor Array with Multiplexed Detection of Tactile Pressure and Skin Temperature. *Nat. Commun.* **2018**, *9*, 2458.
- (8) Harada, S.; Kanao, K.; Yamamoto, Y.; Arie, T.; Akita, S.; Takei, K., Fully Printed Flexible Fingerprint-Like Three-Axis Tactile and Slip Force and Temperature Sensors for Artificial Skin. *ACS Nano* **2014**, *8*, 12851-12857.